

Mattia Moroder

**Simulation of Electron Energy
Loss Spectroscopy for a MgO
Nanocube by Molecular Dynamics**

Bachelor Thesis



Department of Physics

Karl Franzens University of Graz

Supervisor: Ao. Univ. Prof. Dr. Ulrich Hohenester

June 2018

Abstract

Electron Energy Loss Spectroscopy EELS is a technique that has proven very useful for exciting and mapping plasmons in metallic nanoparticles and phonons in ionic nanoparticles. A monochromatic, atom-wide electron beam passes through or near a probe. This bachelor thesis deals with EELS of a magnesium oxide nanocube. A swift electron couples with phonon vibrations of the probe. The experiments are simulated by means of Molecular Dynamics MD. A Matlab program calculates and plots the swift electrons' energy loss probability for a specific position of the electron beam. The calculations of the interionic forces base on a particle-particle-particle-mesh algorithm P^3M , whose computing time scales linearly with the number of unit cells of the crystal n .

The results of the simulations, in good agreement with those previously obtained by Dr. Hohenester and Dr. Trügler [4],[9], show a slight dependence of the vibrational behavior of the probe from the size of the nanocube.

Declaration

I declare that I have developed and written the enclosed Bachelor Thesis completely by myself, and have not used sources or means without declaration in the text. Any thoughts from others or literal quotations are clearly marked. The Bachelor Thesis was not used in the same or in a similar version to achieve an academic grading or is being published elsewhere.

Graz, June 2018

Mattia Moroder

Acknowledgements

I want to thank Andreas Trügler for helping me with the simulations for the biggest crystals by running them on the Sauron-Cluster, which is part of the high-performance computing systems of the Karl Franzens University of Graz.

Contents

1	Introduction	6
1.1	Overcoming the diffraction limit of light	6
1.2	EELS of a MgO nanocube and Overview	7
2	Theory and Simulation of EELS	9
2.1	Electron Energy Loss Spectroscopy	9
2.2	Molecular Dynamics	10
2.3	Lattice Dynamics and Local Dielectric Description	11
2.3.1	Lattice Dynamics	11
2.3.2	Local Dielectric Description	11
3	Software Description	12
3.1	The P³M Algorithm	12
3.2	The demoverlet.m File	14
3.3	Restrictions to the input parameters	17
4	Data Evaluation	18
4.1	Increasing the size of the crystal for a fixed impact parameter	19
4.2	Varying the impact parameter	21
5	Applications	25
5.1	Nanoscale heat transport and thermoelectrics	25
5.2	Acoustic invisibility cloaks by metamaterials	26
6	Conclusions	28

Chapter 1

Introduction

1.1 Overcoming the diffraction limit of light

As indicated by the word "micro" itself, it is not possible to observe nanostructures using an optical microscope. Its resolution is fundamentally limited to approximately half of the wavelength of the incident light, corresponding to about 250 nm, because of the diffraction limit of light. This represents also the lower limit for light confinement. Fortunately, a way for circumventing the latter obstacle has been discovered.

Under specific circumstances, light waves directed at the interface between a metal and a dielectric can induce a resonant interaction with the the nearly free conduction electrones at the surface of the metal. These coherent charge-oscillations are called surface plasmons. This phenomenon is enhanced in nanoparticles and represents a way for confining light at the nanoscale.

The applications of plasmonics are numerous, ranging from more efficient computer chips to cancer treatment [2]. Nevertheless, visualizing plasmons by optical means is not possible. For this purpose, electrons, which are also able to excite surface plasmons in nanoprobe, are used instead of photons. Electron Energy Loss Spectroscopy EELS (a subfield of electron microscopy) can be schematically described as follows: 1) an atom-wide, nearly monochromatic electron beam passes through or near a nanoprobe, 2) the swift electrons excite plasmons by performing work against the electric field of the probe, 3) by raster scanning the beam over the probe the electron energy loss probability is measured and the shape of the plasmonic modes can be determined.

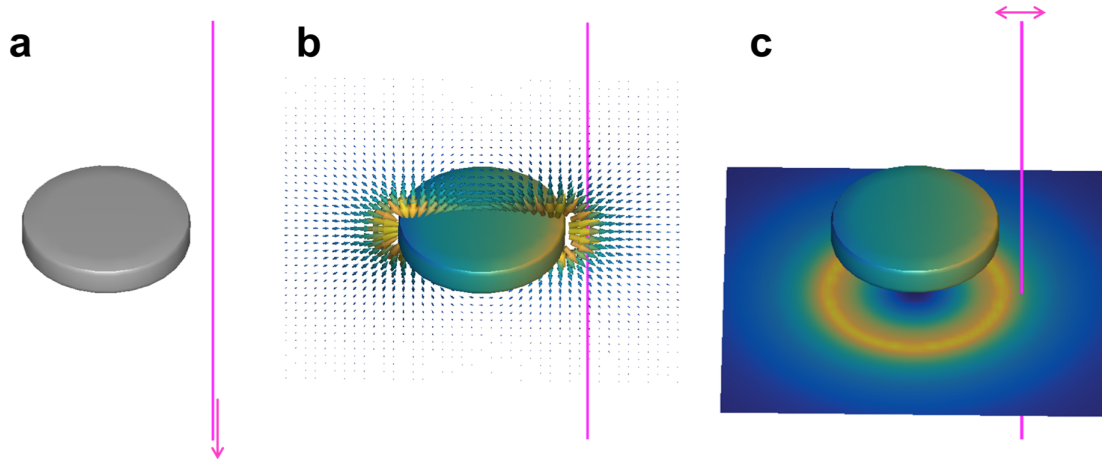


Figure 1.1: Schematic description of EELS for a metallic nanoparticle. a) the swift electron (magenta line) passes near the nanoprobe, b) it excites plasmons, c) the shape of the plasmonic modes is determined by raster scanning the beam over the probe and measuring the electron energy loss probability. Taken from [3].

In ionic crystals, there is no free electron gas that can swing resonantly with an external electric field. Instead, the swift electrons can bring the ions of the crystal to oscillate and this results in phonon modes, with wavelengths typically belonging to the infrared domain. This is also of great interest because understanding phonon transport at the nanoscale is fundamental for many technological applications, like building efficient thermoelectric devices, acoustic cloaking and many others [5]. This work deals with phonon excitation in a Magnesium oxide nanocube.

1.2 EELS of a MgO nanocube and Overview

Electron Energy Loss Spectroscopy presents a lot of experimental difficulties, but recently there have been many improvements (like the development of a new generation of monochromators) and M.J. Lagos and P.E. Batson [9],[4] have been able to spatially map both surface and bulk vibrations in a single magnesium oxide nanocube.

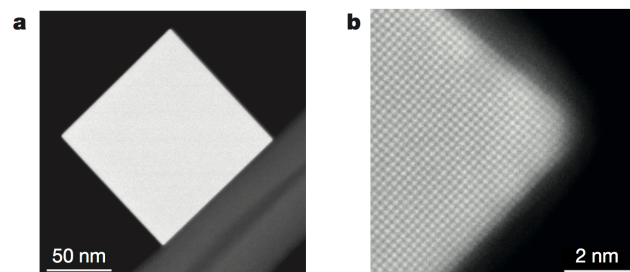


Figure 1.2: a) annular dark field (ADF) image obtained with a scanning transmission electron microscope (STEM) of a 150-nm MgO cube. b) High-resolution ADF image of a cube; the corners and edges are round. There is also a 1–2 nm in thick coating layer. Taken from [4].

The spatial resolution of the beam amounts to 1.5-2 Angstrom and the energy losses of the electrons due to inelastic scattering were determined with a precision of 10 meV.

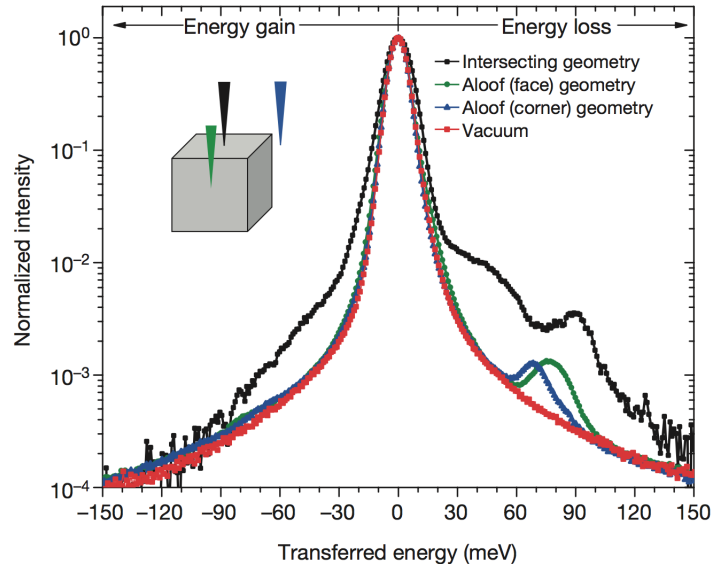


Figure 1.3: Normalized spectra acquired with the electron beam located in different positions: green, the beam is located near a face; blue, the beam is located near a corner; black, the beam passes through the probe. The red dots represent a zero-loss peak (ZLP) profile, acquired in a vacuum. Regions with positive values represent energy loss and regions with negative values represent energy gain. Taken from [4].

The green, blue and black peaks in fig.1.3 correspond to the various phonon modes of the probe.

For simulating the experiment, several techniques have been used. The one that will be presented in this work is the Molecular Dynamics (MD) technique. I used a program previously written by Ulrich Hohenester and Andreas Trügler for simulating larger nanocubes (number of unit cells $n = 64$) than those that were previously simulated ($n_{max} = 32$) in order to analyze whether/how the dimension of the cube affect its vibrational modes and also for coming closer to the size of the cubes used in the experiments ($n > 240$).

This work is organized as follows:

- In Chapter 2 the formula for the electron energy loss probability is derived and the MD method is explained. The latter is then compared with the Lattice Dynamics (LD) and Local Dielectric Description (LDD) methods.
- In Chapter 3 the software used for the MD simulation is described together with the applied Particle-Particle-Particle-Mesh (P^3M) algorithm.
- In Chapter 4 I present and analyze my results and compare them with the ones of ref.[9] and [4].
- In Chapter 5 I point out some technological applications that base on phonon-controlling at nanoscales.
- In Chapter 6 I discuss my results.

Chapter 2

Theory and Simulation of EELS

2.1 Electron Energy Loss Spectroscopy

As we have seen, what is needed for describing the vibrational behavior of the nanoprobe is a formula for the electron energy loss probability. The derivation of the formula follows [3] and [9], in which Gaussian units are used.

This formula describes the probability for a swift electron to lose a certain amount of energy, due to interactions with the probe. These losses can then be interpreted as bulk or surface, phonon or phonon-polariton excitations. The ions in the MgO crystal (Mg^{2+} and O^{2-}) are described as point-like particles carrying an effective charge. The second assumption made is that the thermal energy is zero i.e. that the ionic system resides in its ground state.

The schematic steps of the electron energy loss spectroscopy are shown in fig.1.1. We label $\mathbf{r}_e(t)$ the position of the electron and $\mathbf{E}[\mathbf{r}_e(t)]$ and $\mathbf{B}[\mathbf{r}_e(t)]$ respectively the electric and the magnetic field at this position. Note that $\mathbf{E}[\mathbf{r}_e(t)]$ does not include the field generated by the electron itself. By expressing the infinitesimal propagation distance as $d\mathbf{l} = \mathbf{v}dt$ we can write the work performed by the swift electron against the electric field as:

$$dW = -e(\mathbf{E}[\mathbf{r}_e(t)] + \mathbf{v} \times \mathbf{B}[\mathbf{r}_e(t)]) \cdot \mathbf{v}dt = -e\mathbf{E}[\mathbf{r}_e(t)] \cdot \mathbf{v}dt \quad (2.1)$$

Here e is the elementary electrical charge. We can see that the magnetic field cannot perform work because $(\mathbf{v} \times \mathbf{B}) \cdot \mathbf{v}$ is always equal to zero. The total amount of energy lost by the electron is then calculated by integrating over its entire trajectory,

$$\Delta E = e \int_{-\infty}^{\infty} \mathbf{E}[\mathbf{r}_e(t)] \cdot \mathbf{v}dt \quad (2.2)$$

We assume that the trajectory of the electron, because of its large kinetic energy (typically of the order of 100 keV), is not influenced by the field of the probe. For an electron traveling in the positive z-direction, we can write its trajectory as

$$\mathbf{r}_e(t) = \mathbf{R}_0 + \hat{\mathbf{z}}vt \quad (2.3)$$

with $\mathbf{R}_0 = (x_0, y_0)$ being the impact parameter. Actually, in the experiment, the energy losses are calculated by measuring the electrons' velocity changes at the detector, but in the theoretic model those losses are already described in eq.2.2. We can decompose ΔE into its frequency components via Fourier transform:

$$\mathbf{E}(\mathbf{r}, t) = \int_0^{\infty} e^{-i\omega t} \mathbf{E}(\mathbf{r}, \omega) \frac{d\omega}{2\pi} \quad (2.4)$$

with ω being the angular frequency. The last thing we need to do is to decompose ΔE into loss contributions $\hbar\omega$ and assign to every loss energy $\hbar\omega$ a loss probability Γ_{EELS} .

$$\Delta E = \int_0^\infty \hbar\omega \Gamma_{EELS}(\mathbf{R}_0, \omega) d\omega \quad (2.5)$$

Now by inserting eq.2.4 into eq.2.2 we get

$$\Gamma_{EELS}(\mathbf{R}_0, \omega) = \frac{e}{\pi\hbar\omega} \int_{-\infty}^\infty \Re\{e^{-i\omega t} \mathbf{v} \cdot \mathbf{E}(\mathbf{r}_e, \omega)\} dt \quad (2.6)$$

For the upcoming calculations it is convenient to express the EELS probability as function of the induced polarization current in the crystal \mathbf{J}_{ind} .

$$\Gamma_{EELS}(\mathbf{R}_0, \omega) = \frac{1}{\pi\hbar\omega} \int \Re[\mathbf{E}_{el}^*(\mathbf{r}, \omega) \cdot \mathbf{J}_{ind}(\mathbf{r}, \omega)] d^3r \quad (2.7)$$

In the next section, I will describe the MD technique and how it allows calculating \mathbf{J}_{ind} .

2.2 Molecular Dynamics

Substantially, for our case with the MD technique we want to solve Newton's equations of motion for the crystal's ions when the swift electrons pass by in order to calculate the induced polarization current \mathbf{J}_{ind} .

First of all, the ground state of the crystal has to be computed by relaxation. As mentioned before, the ions are represented as point-like particles, with masses M_j and charges eZ_j at the positions \mathbf{R}_j . In practice, it is impossible to account for the exact interaction of every ion with all the other ones, since this task becomes computationally prohibitive already for a small number of ions. Instead, a Particle-Particle-Particle-Mesh algorithm (P^3M), in which the interactions are divided into interatomic forces (for near ions) and smooth Coulomb forces for distant ions, is applied. This algorithm will be described in sec.3.1. Here I only want to mention that it allows an accurate interionic force calculation and that the computing time scales linearly with the number of ions.

The equations of motion have the following shape

$$M_j \ddot{\mathbf{R}}_j + \nabla_{\mathbf{R}_j} \sum_{j'} V_{jj'}(\mathbf{R}_j - \mathbf{R}_{j'}) - \gamma M_j \dot{\mathbf{R}}_j = eZ_j \mathbf{E}_{el}(\mathbf{R}_j, t) \quad (2.8)$$

Here the force splitting isn't explicitly given, it is contained in $V_{jj'}$, the potential between two ions j and j' . The last term of the lefthand side of the equation is a dissipative term, which accounts for various couplings with the environment, like small thermal excitations. To solve these equations, a Verlet algorithm [17] with a time step of 1 fs is used. Once the ion trajectories have been obtained, the induced polarization current can be expressed as follows

$$\mathbf{J}_{ind}(\mathbf{r}, t) = \sum_j \dot{\mathbf{R}}_j eZ_j \delta(\mathbf{r} - \mathbf{R}_j) \quad (2.9)$$

Finally we can compute the Fourier Transform of the induced current

$$\mathbf{J}_{ind}(\mathbf{r}, \omega) = \int_0^\infty \mathbf{J}(\mathbf{r}, t) dt \quad (2.10)$$

and insert it into Eq. 2.7 to calculate the electron energy loss probability.

2.3 Overview of Lattice Dynamics and Local Dielectric Description

In this section, the basic ideas underlying two alternative/complementary techniques for simulating the EELS experiment will be pointed out. I will be brief because my work mainly deals with MD. Both techniques are exhaustively described in [9].

2.3.1 Lattice Dynamics

The main difference between MD and Lattice Dynamics LD is that in the latter the probe is approximated by an infinite crystal. In this way no surface effects have to be considered and it's possible to exploit the perfect symmetry of the crystal for the calculations, lowering considerably the computational effort, in comparison to MD. One of the disadvantages of LD is that of course excitations occurring on the surface of the crystal cannot be reproduced.

Both MD and LD are useful descriptions for the case in which the beam passes through the crystal (intercepting geometries). In cases in which the beam passes near the probe (aloof geometries), the Local Dielectric Description can be applied.

2.3.2 Local Dielectric Description

The idea is to find a dielectric description of the MgO probe and then to solve Maxwell's equations for the quasistatic approximation (see the appendix). One possibility is to use a Lorentzian oscillator model

$$\epsilon(q \rightarrow 0, \omega) = \epsilon_\infty \left[1 + \frac{\omega_{LO}^2 - \omega_{TO}^2}{\omega_{TO}^2 - \omega(\omega + i\eta)} \right] \quad (2.11)$$

Here ω_{TO}^2 and ω_{LO}^2 are the frequencies of the transversal and the longitudinal optical phonons respectively, ϵ_∞ the high-frequency permittivity of the crystal and η a damping constant. An additional term has to be introduced for describing bulk losses.

The reason this description doesn't work well for intersecting geometries is that the long wavelength approximation doesn't account for short-wave phonon excitations.

Chapter 3

Software Description

3.1 The P³M Algorithm

As explained in sec 2.2, in the MD method we want to calculate the motion of the crystal's ions by solving Newton's equations of motion. For such many-particle problems, the Particle-Particle-Particle-Mesh (P^3M) algorithm is very convenient. A comprehensive explanation of the P^3M algorithm can be found in [7]. It is a combination of the particle-particle (PP) and the particle-mesh (PM) algorithms.

In the PP algorithm, all the forces between the particles are computed one by one. This is conceptually easy but computationally impracticable. In fact the CPU time scales with $10N_p^2$, with N_p being the total number of considered particles.

In the PM algorithm, the interactions between the particles are described by a smooth potential, which is defined only on certain discrete mesh points. This mesh is called the charge-potential mesh. The forces are computed by deriving the mesh-defined potential with respect to the position variable and by interpolating on the particle positions. This method is computationally less demanding than the PP method, but also less accurate.

In the P^3M algorithm we want to combine the high precision of PP with the high speed of PM. The particles' trajectories are integrated forwards in time using the leapfrog scheme [11]:

$$\mathbf{x}_i^{n+1} = \mathbf{x}_i^n + \frac{\mathbf{P}_i^{n+1/2}}{m_i} DT \quad (3.1)$$

$$\mathbf{P}_i^{n+1/2} = \mathbf{P}_i^{n-1/2} + (\mathbf{F}_i)DT \quad (3.2)$$

Here \mathbf{x}_i^n and \mathbf{P}_i^n are the position and the momentum, respectively, of the i -th particle at the time step n and DT is a discrete time difference.

As anticipated, the force gets split in a short-range force and a long-range, smooth varying force (see the appendix for a simple example of force-splitting).

$$\mathbf{F}_i = \mathbf{F}_i^{sr} + \mathbf{F}_i^m \quad (3.3)$$

The key point here is obviously to find an optimal balance between the PP and the PM contributions.

We define a certain cutoff radius r_e and establish that only particles whose distance is smaller than r_e contribute to \mathbf{F}_i^{sr} . Both the CPU time and the accuracy are proportional to the magnitude of r_e . For a two-dimensional particle distribution,

finding which particles contribute to \mathbf{F}_i^{sr} would require N_p^2 tests. In order to overcome this problem, a second mesh, called chaining mesh, is used. The side of the chaining mesh is usually three-four times larger than the one of the charge-potential mesh. Typical relative sizes of r_e , the charge-potential mesh and the chaining mesh are represented in the image below.

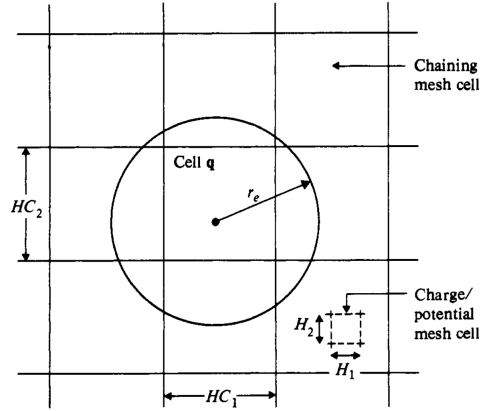


Figure 3.1: Representation of typical relative sizes of the cutoff radius r_e , the charge-potential mesh and the chaining mesh. Taken from [7].

From this picture, we can see that particles contributing to \mathbf{F}_i^{sr} have to be searched only inside the central cell q and in the eight cells adjacent to it. This means that for finding those particles we have to perform only $9N_C N_p$ tests, with N_C being the number of particles contained in one cell. This is much less than N_p^2 tests because $N_C \ll N_p$. Exploiting Newton's third law this number can be halved. The same procedure for three dimensions leads to $N_{tests} \simeq 13N_C N_p$. A scheme of the P^3M algorithm is presented in the figure below.

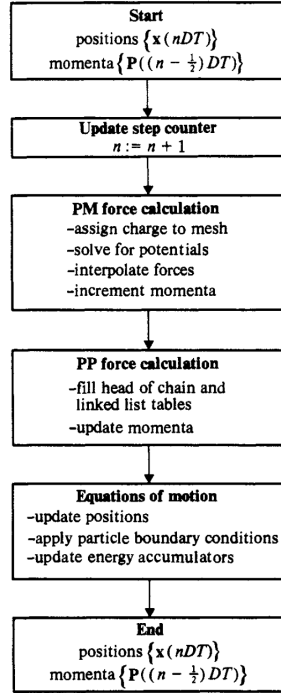


Figure 3.2: schematic representation of the key steps of the P^3M Algorithm. Taken from [7].

Overall, the CPU time for the P^3M algorithm scales linearly with the number of simulated particles.

3.2 The demoverlet.m File

In this section, the Matlab file "demoverlet.m" used for the MD simulation will be presented and explained. It computes and plots the electron energy loss probability for the electron beam passing at a specific position. This main file calls many functions defined in other files, and that allows this relatively complex program to occupy less than 70 lines. I will use parentheses for referring to a specific code line, for example (2) means line 2.

```

1 % DEMOVERLET1
2
3 atomicunits;
4 % number of units cell for cube
5 n = 4;
6 % MgO cube
7 cube = mgocube( n );
8 % groundstate
9 tol = 1e-4;
10 u0 = groundstate2( cube, tol );
  
```

In this first part of the program, some constants for the use of atomic units are imported (3), the number of unit cells n is chosen (5), the cube is generated (7) and the groundstate u_0 is calculated (10) with a certain tolerance tol (9).

```

11
12 % positions and indices of atoms
13 [ pos, ind ] = full( cube );
14 % mass and charge
15 mass = repmat( reshape( cube.m( ind ), [], 8 ), 1, 1, 3 );
16 q = reshape( cube.q( ind ), [], 8 );
17 % impact parameter
18 imp = ( 0.25 * [ 1, 1 ] + n / 2 * [ 1, 1 ] ) * cube.a0 * bohr;
19 % electron beam
20 beam = electronbeam( imp / bohr );
21 % electron velocity (atomic units)
22 vel = beam.vel / fine;
23 % electric field of electron beam
24 e = efield0( beam, reshape( pos + u0, [], 3 ) ) / vel;
25 frc = reshape( bsxfun( @times, e, q( : ) ), size( pos ) );
26
27 % plotting of cube and impact parameter
28 % you may like to comment the following lines
29 plot( cube, u0 ); hold on
30 plot3( imp( 1 ), imp( 2 ), max( pos( :, 3 ) ) * bohr + 0.1, 'k+' );
31 view( 0, 90 );

```

The most important part of this code lines is the choice of the impact parameter (18), which is the position at which the beam passes. With this input, the electric field of the beam is calculated (24). Finally, a slice of the crystal orthogonal to the beam is plotted together with the impact parameter (29-31).

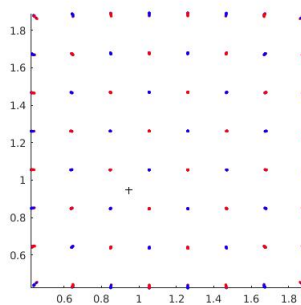


Figure 3.3: Crystal lattice plotted for $n = 8$ and the beam (depicted by the cross symbol) passing through the middle of a cell. The blue dots represent the magnesium atoms and the red dots the oxygen atoms.

```

32 % time step
33 % 1 fs, see Chalopin et al., Appl. Phys. Lett. 100, 241904 (2012).
34 dt = 1 / tunit;
35 % loss energies and damping
36 ene = linspace( 20, 120, 200 ) * 1e-3 / hartree;
37 gamma = 2e-3 / hartree;
38
39 % number of time steps
40 nit = 2500;
41 time = ( 1 : nit ) * dt;
42 % allocate output
43 vv = zeros( size( time ) );
44
45 % initial displacements and velocities

```

3.2. THE DEMOVERLET.M FILE

```

46 [ u, v ] = deal( u0, frc ./ mass );
47 a = force( cube, u ) ./ mass;

```

In this part, the time steps for Newtons' equations are chosen (34), together with a damping term accounting for interactions with the environment (37). The energy range for which the EELS probability should be calculated is also defined (36). Eventually, the initial displacements and velocities are set up (46-47).

```

48 multiWaitbar( 'Verlet', 0, 'Color', 'g' );
49 % Verlet loop
50 for it = 1 : nit
51 % update displacement
52 u = u + v * dt + 0.5 * ( a - gamma * v ) * dt ^ 2;
53 v = v + 0.5 * ( a - gamma * v ) * dt;
54
55 % update velocity
56 a = force( cube, u ) ./ mass;
57 v = ( v + 0.5 * a * dt ) / ( 1 + 0.5 * gamma * dt );
58
59 vv( it ) = sum( frc( : ) .* v( : ) );
60
61 if mod( it, 50 ) == 0, multiWaitbar( 'Verlet', it / nit ); end
62 end
63 % close waitbar
64 multiWaitbar( 'CloseAll' );

```

Here Newton's equations are solved for obtaining the trajectories of the particles, accounting for the force generated by the polarization current induced by the beam (50-57). Additionally, a wait bar showing the progress of the calculation with a step of 2% is set up (48,61) and closed at the end of the process (64).

```

65 figure
66
67 prob = real( vv * exp( li * time( : ) * ene ) * dt ) ./ ( pi * ene *
    hartree );
68 plot( ene * hartree * 1e3, prob ); hold on

```

Finally, with the results of the calculations performed above, the electron energy loss probability (formula 2.7)) is computed (67) and plotted for energies between 20 and 120 meV (68).

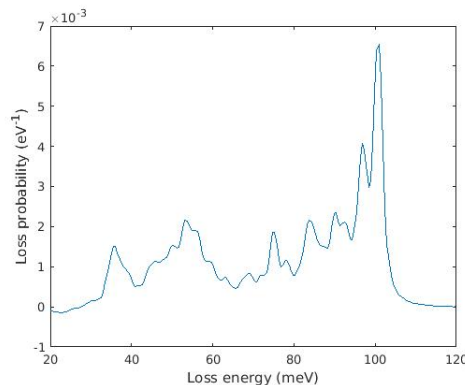


Figure 3.4: a output plot of the EELS probability for $n = 4$

3.3 Restrictions to the input parameters

As discussed in sec.2.2, a rigid ion approximation is applied. This approximation is valid only if the beam doesn't pass too close to an atom, because in that case, the electron "feels" the whole charge of the atom and not only its effective charge.

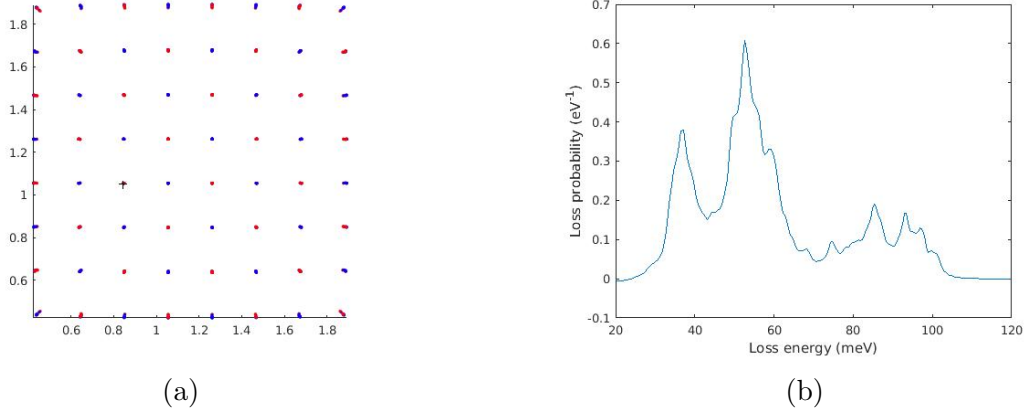


Figure 3.5: (a) Lattice with beam passing too close to an oxygen atom. (b) Corresponding EELS probability

Another aspect to be considered when choosing the impact parameter is that the beam should pass through the crystal and not near it (for aloof geometries a LDD is used, see sec. 2.3.2). I also found that, in order to get meaningful results (at least according to the interpretation of the EELP peaks given in [9]), the beam should pass through one of the central unit cells.

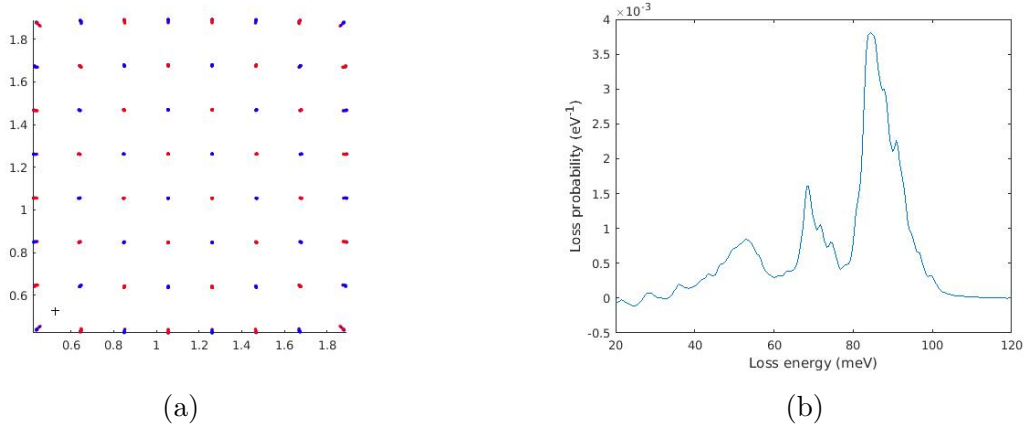


Figure 3.6: (a) Lattice with beam passing through the middle of a unit cell located in a corner of the crystal. (b) Corresponding EELS probability.

Chapter 4

Data Evaluation

First of all, I have checked whether the computational time scales linearly with the number of atoms in the crystal, as we would expect from the P^3M algorithm. This, of course, corresponds to an n^3 scaling, since the crystal is three-dimensional.

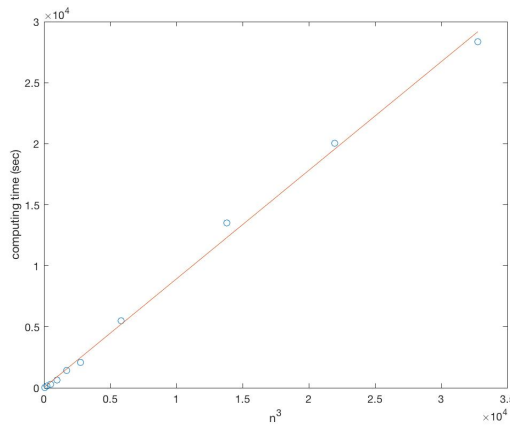


Figure 4.1: computing time as a function of n^3 . The circles represent the measured times and the red fit shows the linear growth. The last dot right corresponds to $n=32$.

Following [9], I will interpret the electron energy loss probability peaks between 35 meV and 50 meV as acoustic phonon excitations, those between 60 and 80 meV as lying in the reststrahlenband of the MgO cube associated with surface phonon polaritons excitation and those above 80 meV as excitations of optical phonons (see the glossary). For simplifying comparisons, I have chosen the same labeling for the impact parameters as in [9].

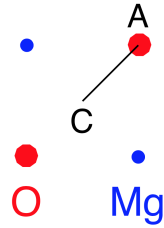
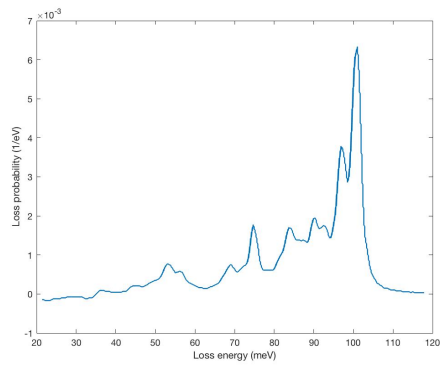


Figure 4.2: impact labeling. The center of the crystal cell correspond to the impact parameter = C. Taken from [9].

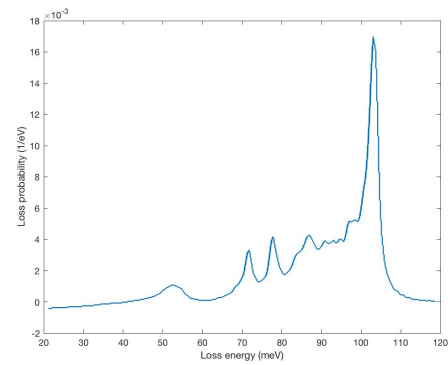
4.1 Increasing the size of the crystal for a fixed impact parameter

I have chosen C (the center of the crystal cell) as the impact parameter and have run the simulation for $n = 4$, $n = 8$, $n = 16$, $n = 32$ and $n = 64$. The results are shown below.

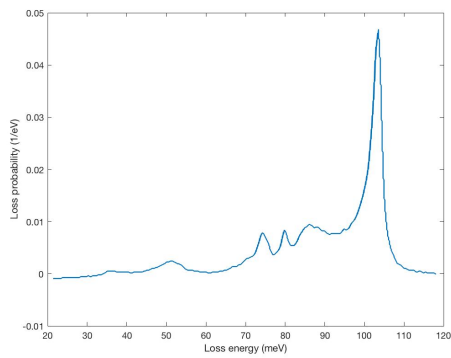
4.1. INCREASING THE SIZE OF THE CRYSTAL FOR A FIXED IMPACT PARAMETER



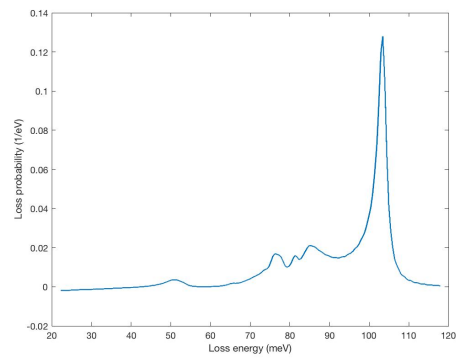
(a) $n = 4$



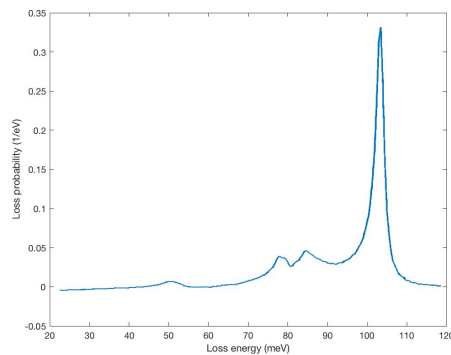
(b) $n = 8$



(c) $n = 16$



(d) $n = 32$



(e) $n = 64$

Figure 4.3: plots of the swift electrons' energy loss probability for five different sizes of the crystal

We can note a slight decrease of all the peaks when increasing the size of the crystal, except for the one at about 105 meV. This means that the optical phonons get more predominant for big crystals. Of course, the overall energy loss probability is bigger for bigger crystals, since there are more ions the swift electron can interact with. What is relevant though is the relative height of the peaks to one another. I have plotted these 5 results together.

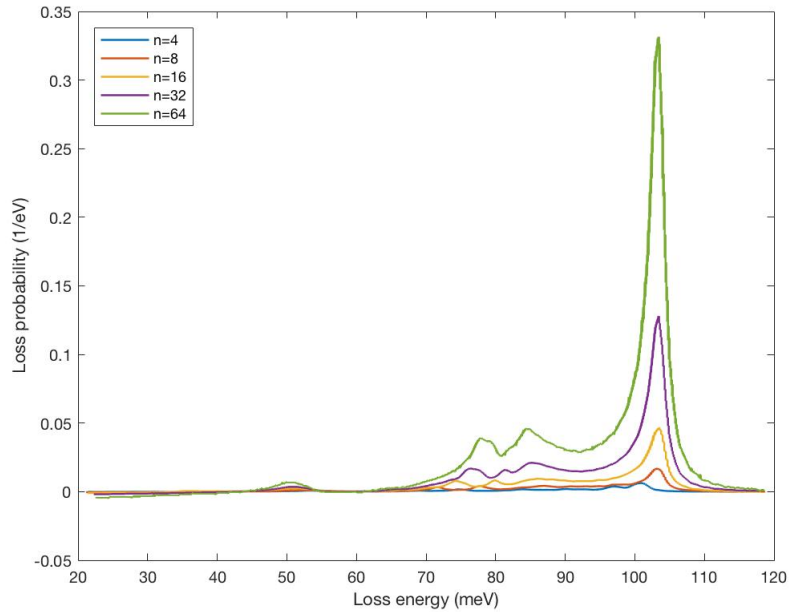


Figure 4.4: combination of the five plot shown in fig. 4.3.

This plot can be misleading if we look at the peaks below 100 meV, which seem to increase with the size of the crystal (which they actually don't, as explained above and can be seen in fig.4.3). What this plot shows us, is that the energy at which the main peak occurs is the same for every crystal size, at about 105 meV. This, according to the interpretation given in ref.[9], means that, independently from the crystal's size, optical phonons with an eigenenergy about 105 meV will be excited.

4.2 Varying the impact parameter

We have already seen how the size of the crystal affects energy loss probability for the beam passing at the center of the crystal cell. Now I want to investigate those effects for different impact parameters. This had already been done in ref.[9] and I report their result below.

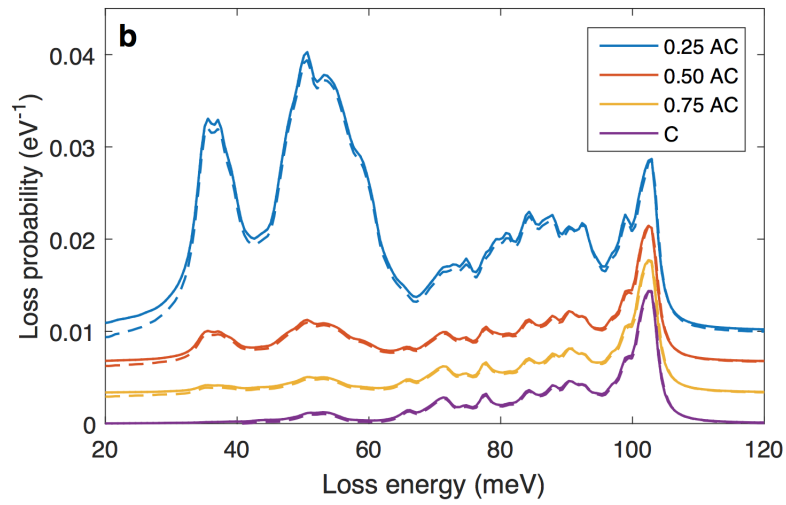


Figure 4.5: swift electrons' energy loss probability for 4 different impact parameters for $n=8$, done by Hohenester et al. Taken from [9].

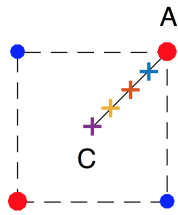
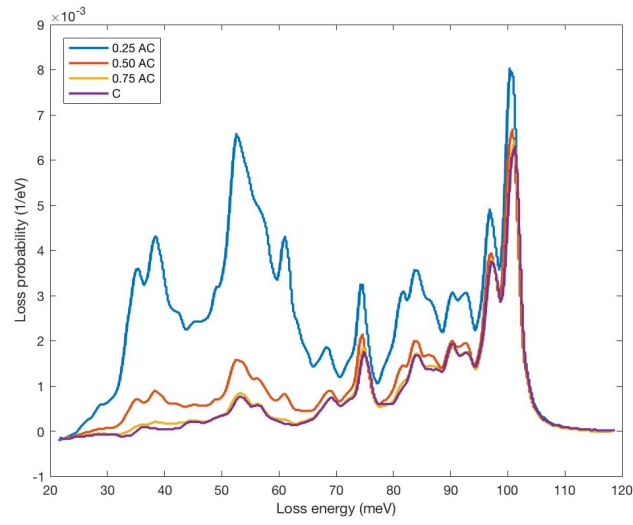


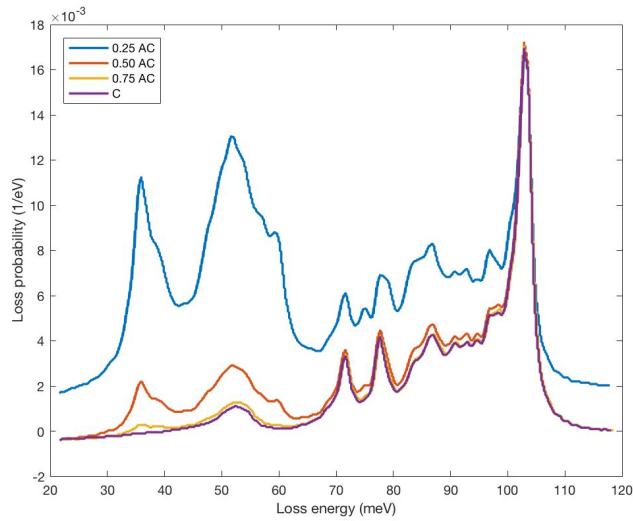
Figure 4.6: chosen impacts. Taken from [9].

I have run the simulations for the same impact parameter but for the following sizes of the crystal: $n = 4, 8, 16$. The results are shown below.

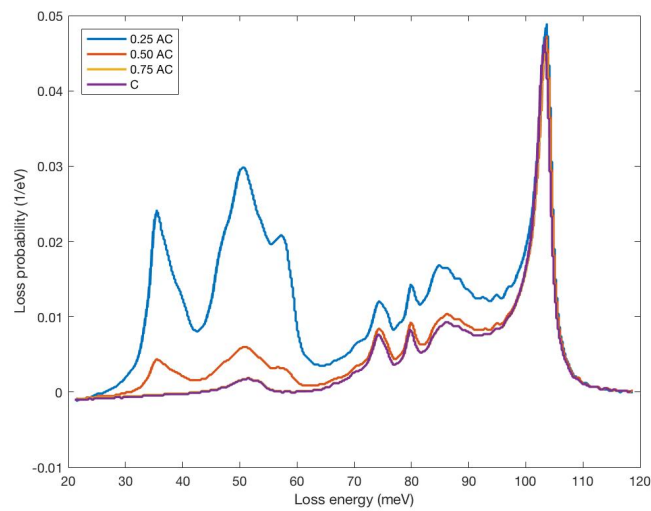
4.2. VARYING THE IMPACT PARAMETER



(a) $n = 4$



(b) $n = 8$



(c) $n = 16$

Figure 4.7: swift electrons' energy loss probability for 4 different impact parameters and 3 different sizes of the crystal.

From this plots we can see that, as was found in [9], the closer the beam gets to an ion, the more energy losses between around 30 and 90 meV are detected. These 3 plots also seem to show that the crystal's size doesn't strongly influence its vibrational behaviour. Nevertheless, for $n = 16$ the peaks between 60 and 80 meV are somewhat smaller than they are for $n = 4$ and $n = 8$. Recall that these correspond to phonon polariton excitations localised on the surface of the cube. It sounds reasonable that, as the surface/volume ratio of the crystal decreases (by raising n), also the surface excitations lose importance. This seems to hint that, for large crystals, the MD and LD (in which no surface excitations can be accounted for) results tend to converge, at least to a certain extent. This doesn't mean that surface phonon polariton excitations are negligible for the crystals used in experiments ($n > 240$); in fact they have been found also experimentally [9],[4]. It only seems to justify the use of LD.

Chapter 5

Applications

For this chapter, I will use [5] as my main source.

The purpose of the EELS is to determine the vibrational behavior of different probes. But why is this important?

In ref.[5], Maldovan points out, that the great technological development that has occurred in the last decades is mainly based on our ability to control electrons and photons. Being able to manipulate phonons, the particles associated with mechanical vibrational energy, in a similar way, would give a new push to technological innovation.

Phonons are responsible for both the transmission of sound and heat. The main difference between this two everyday phenomena is that heat is characterized by high frequencies and short propagation distances, while by contrast sound waves have low frequencies and can cover long distances.

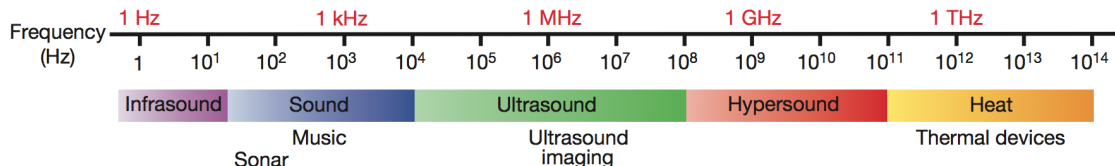


Figure 5.1: scale of the frequencies of sound and heat. Taken from [5].

Let's now have a look at two interesting innovations based on phonon control.

5.1 Nanoscale heat transport and thermoelectrics

Thermoelectrics are materials that can convert heat into electricity. They are of great importance since by turning waste thermal energy into valuable electric energy they represent an alternative source of energy for the future. The efficiency of thermoelectric materials is measured by the so-called thermoelectric figure of merit $ZT = S^2\sigma T/\kappa$. Here S is the Seebeck coefficient (see the glossary), σ the electric conductivity, T the temperature and κ the thermal conductivity. From this formula, we can deduce that in order to enhance thermoelectrical properties the thermal conductivity has to be reduced. This can be achieved by adding interfaces at which phonons get scattered, which limits their ability to propagate. Various nanostructures have proven themselves as very useful for accomplishing phonon scattering. In

[1] for example, ErAs nanoparticles were placed into $In_{0.53}Ga_{0.47}As$, a semiconductor crystal and the thermal conductivity was reduced by a factor of 2.

The EELS technique allows optimizing the shapes and dimensions of nanomaterials in order to make them exhibit low phonon excitations when current flows through them. This is exactly what is needed for manufacturing highly efficient thermoelectrics.

5.2 Acoustic invisibility cloaks by metamaterials

Acoustic cloaking means rendering an object invisible to sound waves. This means that the propagation of the sound waves should not be affected by the object it hits i.e. the incoming waves should be restored at the back of the object.

For achieving this, the object must be surrounded by an engineered metamaterial (see the glossary), which is in general difficult to manufacture. One way to develop such a material is to exploit the similarities between sound waves and electromagnetic waves. The propagation of electromagnetic waves on transmission lines can be described by the telegrapher's equations [16]. According to this equations, the wave patterns are dependent on the inductances and capacities they encounter. Following this so-called LT (line transmission) model, an aluminium plate, consisting of 16 homogeneous concentric cylinders was used as an acoustic cloaking shell by Zhang et al., [8]. It is shown in the image below.

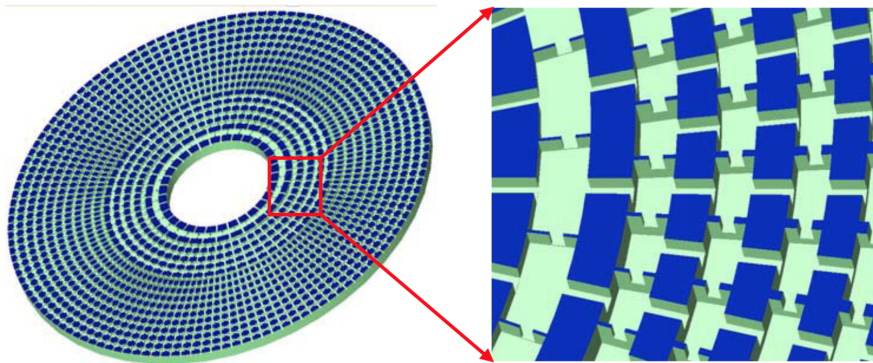


Figure 5.2: Configuration of the acoustic cylindrical cloak synthesized by an acoustic transmission line, namely, inductors and capacitors. Taken from [8].

The cavities act like acoustic capacitors and the connecting channels as acoustic inductances. A probe surrounded by this cloak was put into water and irradiated by ultrasound frequencies in a range of (40-80 kHz). It was shown that, thanks to the cloak, the waves were restored nearly unaltered.

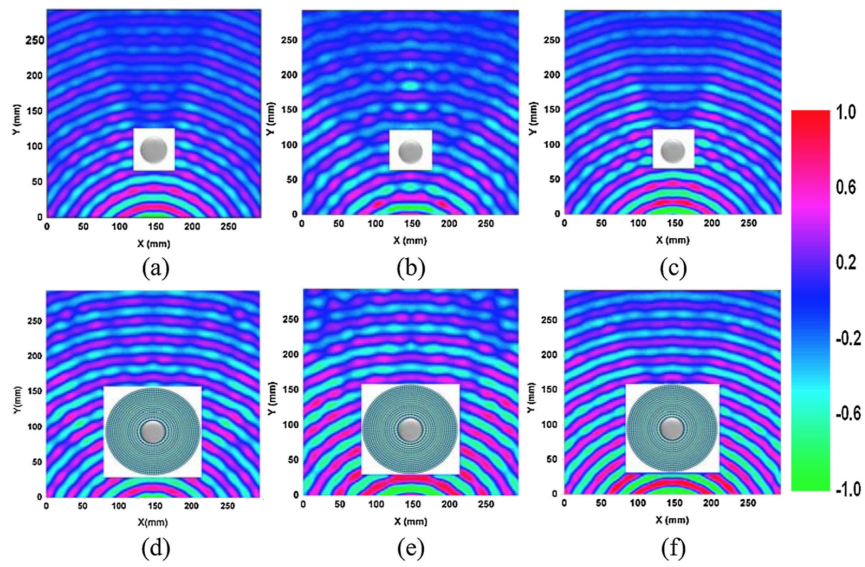


Figure 5.3: The scattering patterns of a mere steel cylinder put in a water tank and illuminated with a point ultrasound source at frequencies of (a) 60 kHz (b) 53 kHz, and (c) 64 kHz. The scattering patterns of a steel cylinder surrounded by the above-described cloak at (d) 60 kHz (e) 52kHz, and (f) 64 kHz. Taken from [8].

Heat cloaking bases on similar principles and is also being developed, as described in [6].

Chapter 6

Conclusions

The Electron Energy Loss Spectroscopy EELS is a powerful method for determining the vibrational behavior of a probe. It can be efficiently be simulated by the Molecular Dynamics method MD based on a Particle-Particle-Particle-Mesh (P^3M) algorithm.

I found that the MD simulation works also for crystals with $n > 32$ and that the CPU time scales linearly with the number of atoms of the crystal (fig.4.1) as expected for the P^3M algorithm. When running the "demoverlet1.m" program, the impact parameter has to be distant enough from the ions (as explained in [9]) and also located in one of the central cells (see sec. 3.3).

The results of sec. 4 are in good agreement with those of [9] and [4],1.3. These show that the vibrational behavior of the MgO nanocube is not strongly dependent on the size of the cube. However, the plots of the EELS probability for $n = 4, 8, 16, 32, 64$ show the general trend of a slight decrease of the peaks up to 80 meV. For the peaks between 60 and 80 meV, this can be interpreted as a consequence of the decrease of the surface/volume ratio of the cube when its size increases.

Appendix

Quasistatic approximation of Maxwell's Equations

The general form of Maxwell's equations in matter is the following:

$$\nabla \cdot \mathbf{D} = \rho_f \quad (1) \quad \nabla \times \mathbf{E} = -\frac{\partial \mathbf{B}}{\partial t} \quad (2)$$

$$\nabla \cdot \mathbf{B} = 0 \quad (3) \quad \nabla \times \mathbf{H} = \mathbf{J}_f + \frac{\partial \mathbf{D}}{\partial t} \quad (4)$$

For static systems, like for steady currents, these equations can be decoupled into electrostatic equations and magnetostatic equations. In cases in which only the change of either the E-field or the B-field are important, we can use the quasistatic approximation of the equations, which are then easier to solve than the full Maxwell equations.

In the electro-quasistatic case (the energy of the E-field is dominant over the energy of the B-field) eq.(2) becomes $\nabla \times \mathbf{E} = 0$.

In the magneto-quasistatic case (the energy of the B-field is dominant over the energy of the E-field) eq.(4) becomes $\nabla \times \mathbf{H} = \mathbf{J}_f$.

Glossary

- **acoustic phonon:** coherent oscillation of the atoms of a crystal around their equilibrium position. The atoms can oscillate parallel to the propagation direction of the phonon, like soundwaves (longitudinal acoustic phonons) or perpendicularly to it, like electromagnetic waves (transverse acoustic phonons), [13].
- **optical phonon:** the name "optical" phonon comes from the fact that in ionic crystals, those type of lattice vibration is excited by infrared radiation. Optical phonons are vibrations in which the neighboring atoms move in opposite directions. They can be excited only if the base of the crystal contains at least two atoms. The adjacent positive and negative ions swinging against each other generate an electric dipole moment which varies in time, [13].
- **polariton:** bosonic quasiparticle arising from the strong coupling of em waves with an excited state (like a phonon), which carries an electric or a magnetic dipole. It should not be confused with a polaron, which is a fermionic quasiparticle. See ref.[14].
- **metamaterial:** material engineered in such way that it gains properties which materials found in nature do not show. Usually, special properties of metamaterials arise from the shape, geometry, orientation, and size of the repeated units they are build of. They are often utilised for manipulating electromagnetic waves or sound waves in devices like for example superlenses or seismic shielding devices, [12].
- **Seebeck coefficient:** indicator of the magnitude of the electric voltage induced in a specific material by a temperature difference as a consequence of the Seebeck effect. Its unit is Volt per Kelvin (V/K). For conductors, the coefficient will be positive if the moving charge-carriers are electron holes and negative if they are electrons, [15].
- **Inelastic scattering:** scattering process in which the kinetic energy of the incident particles is not conserved. Similarly, in mechanical collision processes, inelastic collisions are those in which part of the kinetic energy of the colliding particles is not conserved, for instance because of some dissipative effects. However, inelastic scattering can also arise from an elastic collision, for example in the case of the Compton scattering. When an electron collides with a probe (like in the EELS), most of the scatterings will be elastic and only a small fraction will be inelastic, [10].

Bibliography

- [1] W. Kim et al. “Thermal Conductivity Reduction and Thermoelectric Figure of Merit Increase by Embedding Nanoparticles in Crystalline Semiconductors”. In: *Physical Review Letters* 96, 045901 (2006).
- [2] H. A. Atwater. “The Promise of Plasmonics”. In: *Scientific American* 56 (207).
- [3] Ulrich Hohenester. *Handbook of Metamaterials and Nanophotonics*. to be published. Chap. Plasmon excitation by fast electrons.
- [4] M. J. Lagos et al. “Mapping vibrational surface and bulk modes in a single nanocube”. In: *Nature* 543 (2017).
- [5] M. Maldovan. “Sound and heat revolutions in phononics”. In: *Nature* 503 (2013).
- [6] S. Narayana and Y. Sato. “Heat Flux Manipulation with Engineered Thermal Materials”. In: *Physical Review Letters* 108, 214303 (2012).
- [7] J.W. Eastwood R.W. Hockney. *Computer Simulation Using Particles*. Adam Hilger, 1998.
- [8] N. Fang S. Zhang C. Xia. “Broadband Acoustic Cloak for Ultrasound Waves”. In: *Physical Review Letters* 106, 024301 (2011).
- [9] U.Hohenester et al. “Inelastic vibrational bulk and surface losses of swift electrons in ionic nanostructures”. In: *Phys. Rev. B* 97, 165418 (2017).
- [10] Wikipedia. *Inelastic scattering*. 2017. URL: https://en.wikipedia.org/wiki/Inelastic_scattering.
- [11] Wikipedia. *Leapfrog Integration*. 2017. URL: https://en.wikipedia.org/wiki/Leapfrog_integration.
- [12] Wikipedia. *Metamaterial*. 2018. URL: <https://en.wikipedia.org/wiki/Metamaterial>.
- [13] Wikipedia. *Phonon*. 2018. URL: <https://en.wikipedia.org/wiki/Phonon>.
- [14] Wikipedia. *Polariton*. 2018. URL: <https://en.wikipedia.org/wiki/Polariton>.
- [15] Wikipedia. *Seebeck coefficient*. 2018. URL: https://en.wikipedia.org/wiki/Seebeck_coefficient.
- [16] Wikipedia. *Telegrapher’s equations*. 2018. URL: https://en.wikipedia.org/wiki/Telegrapher27s_equations.
- [17] Wikipedia. *Verlet Integration*. 2018. URL: https://en.wikipedia.org/wiki/Verlet_integration.